Numerical Analysis for Electromigration of Cu Atom

Materials Transactions, Vol. 48, No. 9 (2007) pp. 2513 to 2517

Numerical Analysis for Electromigration of Cu Atom*1

Takenao Nemoto*2, Tutomu Murakawa and A. Toshimitsu Yokobori, Jr.

Tohoku Univ. Graduated School of Engineering, Sendai 980-8579, Japan

The electromigration of Cu interconnection was investigated to solve the Huntigton's equation by numerical analysis. The Cu atoms moved toward anode from cathode and accumulated at the anode end. This result was in good agreement with the result previously derived by our theoretical analysis. The accumulation rate of Cu atoms increased with increasing in current density, but it was not so influenced by temperature.

The characteristic of the rate of electromigration showed a liner relationship with current density and exponential relationship with temperature. This result agreed with the equation experimentally derived by Black. This result proved that numerical analysis of atom transport equation enables to predict of electromigration failure time. [doi:10.2320/matertrans.MRA2007082]

(Received April 10, 2007; Accepted June 27, 2007; Published August 25, 2007)

Keywords: *electromigration, numerical analysis, copper, large scale integration (LSI)*

1. Introduction

The current density in interconnections has been increasing as the number of transistors on an LSI increases. It is reported that the current density reaches to the order of 10^6 A/cm^2 with the LSI products of the latest 65 nm design rule.[1)] Electrons accelerated by an electric field collide against ionized metal atoms as the current density of an interconnection increases, and the failure mode called electromigration (EM) which exchanges momentum of the electron and the atom becomes serious in the LSI products. Much work has been carried out to improve electromigration lifetimes. Cu addition to aluminum alloys has been adapted to improve EM lifetime. One of the present authors and his coworker have reported that "aging technology", which is a thermal treatment at 200–300°C for 0.5 hr–1 hr in addition to the conventional LSI process, makes Cu atoms segregate at Al grain boundaries, and EM lifetime increases by about 10 times to optimize Cu distribution in Al-based interconnections.[2)] Since the path of electromigration is mainly grain boundary, the segregated Cu atom inhibits an intergranular transport. Moreover, replacing Al based interconnection by Cu has been adopted in a mass production line.[3)]

It is also important to establish the technology to evaluate EM lifetime precisely. EM lifetime in the commercial available products is usually guaranteed 10 years, and this is usually determined from acceleration tests at various combinations of temperature and current density.

One of the present authors has reported that an EM acceleration test at less than 250°C avoids microstructural change in the AlCu interconnection and it enables the EM lifetime under conventional LSI usage conditions to be accurately estimated.[4)] While the examination of EM reliability is usually carried out after all LSI processes have been established, it is a serious problem if EM reliability does not pass the final test. Therefore, computer-aided EM simulation is important in predicting EM lifetime during LSI process optimization.

The equation for mass transport by EM has been presented by Huntington *et al.*, as shown in eq. (1).[5)]

$$\frac{\partial C}{\partial t} = D\nabla\left(\nabla C - \frac{eZ^*}{kT}E \cdot C\right), \tag{1}$$

where C is the concentration of atoms, D is the diffusion coefficient, Z^* is the effective atomic number, k is the Boltzman constant and T is the absolute temperature.

Most researchers analyze the mass transport by EM with a solution for only the second term of eq. (1).[6,7)] Authors applied the continuum model of EM and investigated the mathematical analysis of whole of eq. (1)[8)] under steady-state conditions and have consequently reported that eq. (1) expresses the atom and vacancy accumulation by EM successfully. However, this analysis was carried out with an assumption of an equilibrium situation, and cannot represent the time-sequential phenomenon and time to failure by EM. A numerical technique has been developed by authors for the hydrogen embrittlement of steel. Then, in this research, the time sequential change of concentration of vacancies or atoms and the time to failure are investigated by solving eq. (1) in a Cu interconnection using computer simulation by applying a finite difference method.

2. Calculation Methods

2.1 Basic equation

In real LSI devices, defects formed just after fabrication dominate EM failure. Therefore, an initial defect with radius a is considered, as shown in Fig. 1. The coordinates of the stream function potential, ϕ, and velocity function ψ, are introduced in eq. (2).

$$\begin{aligned}\phi &= j\rho\left(r + \frac{a^2}{r}\right)\cos\theta \\ \psi &= j\rho\left(r - \frac{a^2}{r}\right)\sin\theta,\end{aligned} \tag{2}$$

where $E = \nabla\phi$, j is the current density and ρ is the resistivity.

Figure 2 shows the distribution of electric potential around the initial defect. Using eq. (1) and (2), Equation (3) is given using Gauss' law, $\nabla \cdot E = 0$,

*1This Paper was Originally Published in Japanese in J. Japan Inst. Metals **70** (2006) 374.

*2Present Affiliation, Tokyo Electron Limited, Japan

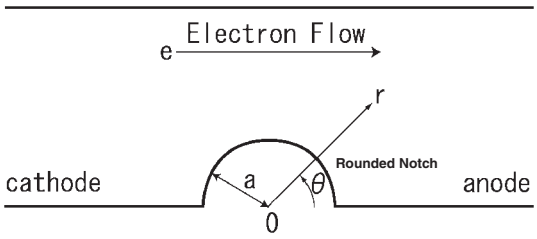

Fig. 1 Model of Analysis.

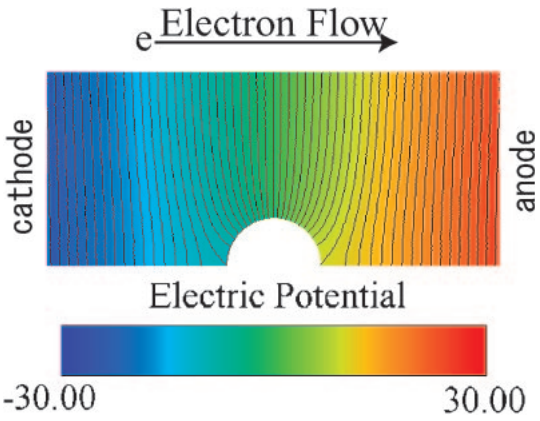

Fig. 2 The potential field ψ around a rounded notch.

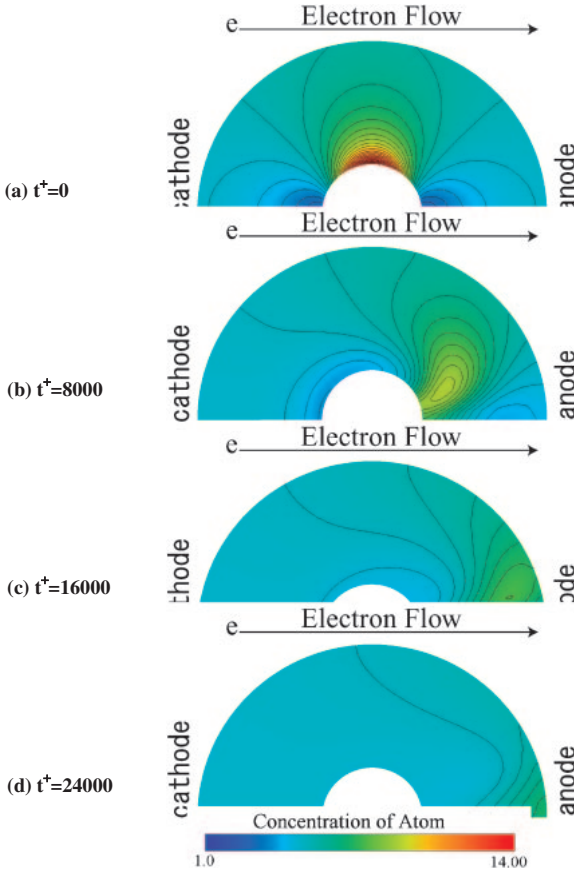

Fig. 3 Time sequential behavior of ionic atom distribution due to electromigration.

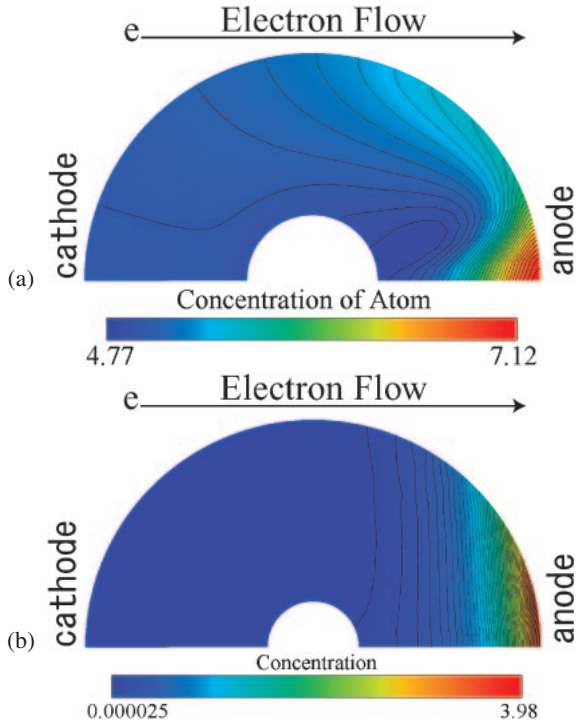

Fig. 4 Comparison of the numerical solution of the transient behavior of electromigration for t $\rightarrow \infty$ (a) with the analysis steady state solution (b).

$$\begin{aligned}\frac{\partial C}{\partial t} &= D\Delta C - \alpha D\frac{eZ^*}{kT}E\cdot\nabla C \\ &= D\frac{\partial^2 C}{\partial r^2} + D\left(\frac{1}{r} - \alpha\frac{eZ^*}{kT}\frac{\partial\phi}{\partial r}\right)\frac{\partial C}{\partial r} \\ &\quad - \alpha D\frac{1}{r^2}\frac{eZ^*}{kT}\frac{\partial\phi}{\partial\theta}\frac{\partial C}{\partial\theta} + D\frac{1}{r^2}\frac{\partial^2 C}{\partial\theta^2}.\end{aligned} \tag{3}$$

2.2 Boundary Condition and Initial Condition

The initial condition is given in eq. (4), and shown in Fig. 4. The diffusing atoms are assumed to be generated at the site of high electric field.

$$C(r,\theta) = \exp\left(\frac{j(r,\theta) - j}{j}\right), \tag{4}$$

where $j(r.\theta)$ is the current density at (r,θ) and $j = \frac{|\nabla\phi|}{\rho}$.

The boundary condition is given in eq. (5). It is assumed that there is no inflow and outflow of atoms occurring at the boundary.

$$\begin{aligned}\left.\frac{\partial C}{\partial r}\right|_{r=0,\max} &= 0 \\ \left.\frac{\partial C}{\partial\theta}\right|_{\theta=0,\pi} &= 0.\end{aligned} \tag{5}$$

2.3 Numerical analysis

A numerical analysis of diffusion has been conducted by the present authors in the case of hydrogen embrittlement cracking of steel.[9] A similar method was applied to the EM atom transport. The non-dimensional values given by eq. (6) are used and eq. (3) is given in eq. (7).

$$r^+ = \frac{r}{a}, \quad C^+ = \frac{C}{C_0}, \quad t^+ = \frac{Dt}{a^2}, \tag{6}$$

$$\begin{aligned}\frac{\partial C^+_{atom}}{\partial t^+} &= \frac{\partial^2 C^+_{atom}}{\partial r^{+2}} + \left\{\frac{1}{r^+} - \alpha a E_0 \frac{eZ^*}{kT}\left(1 - \frac{1}{r^{+2}}\right)\cos\theta\right\}\frac{\partial C^+_{atom}}{\partial r^+} \\ &\quad + \left\{\alpha a E_0 \frac{eZ^*}{kT}\left(\frac{1}{r^+} + \frac{1}{r^{+3}}\right)\sin\theta\right\}\frac{\partial C^+_{atom}}{\partial \theta} + \frac{1}{r^{+2}}\frac{\partial^2 C^+_{atom}}{\partial \theta^2}.\end{aligned} \tag{7}$$

A finite difference version of eq. (7) is written as eq. (8).

$$\begin{aligned}\frac{C^{n+1}_{i,j} - C^n_{i,j}}{\Delta t} &= \frac{1}{2}\left\{\frac{C^{n+1}_{i+1,j} - 2C^{n+1}_{i,j} + C^{n+1}_{i-1,j}}{(\Delta r)^2} + \frac{C^n_{i+1,j} - 2C^n_{i,j} + C^n_{i-1,j}}{(\Delta r)^2}\right\} \\ &\quad + \frac{1}{2}\left\{\frac{1}{r^+} - \alpha a E_0 \frac{eZ^*}{kT}\left(1 - \frac{1}{r^{+2}}\right)\cos\theta\right\}\left(\frac{C^{n+1}_{i+1,j} - C^{n+1}_{i-1,j}}{2\Delta r} + \frac{C^n_{i+1,j} - C^n_{i-1,j}}{2\Delta r}\right) \\ &\quad + \frac{1}{2}\left\{\alpha a E_0 \frac{eZ^*}{kT}\left(\frac{1}{r^+} + \frac{1}{r^{+3}}\right)\sin\theta\right\}\left(\frac{C^{n+1}_{i,j+1} - C^{n+1}_{i,j-1}}{2\Delta\theta} + \frac{C^n_{i,j+1} - C^n_{i,j-1}}{2\Delta\theta}\right) \\ &\quad + \frac{1}{2r^{+2}}\left\{\frac{C^{n+1}_{i,j+1} - 2C^{n+1}_{i,j} + C^{n+1}_{i,j-1}}{(\Delta\theta)^2} + \frac{C^n_{i,j+1} - 2C^n_{i,j} + C^n_{i,j-1}}{(\Delta\theta)^2}\right\},\end{aligned} \tag{8}$$

where,

$$\begin{aligned} r^+ &= i\Delta r^+ \\ \theta &= j\Delta\theta \\ t^+ &= n\Delta t^+, \end{aligned}$$

i, j, n are the node numbers in the radius direction, circumferential direction and time direction, respectively.

Equation (8) can be written as eq. (9).

$$\begin{aligned} &A(r,\theta)C^{n+1}_{i+1,j} + (-1 - B(r,\theta))C^{n+1}_{i,j} + D(r,\theta)C^{n+1}_{i-1,j} \\ &\quad + E(r,\theta)C^{n+1}_{i,j+1} + F(r,\theta)C^{n+1}_{i,j-1} \\ &= -A(r,\theta)C^n_{i+1,j} + (-1 + B(r,\theta))C^n_{i,j} \\ &\quad - D(r,\theta)C^n_{i-1,j} - E(r,\theta)C^n_{i,j+1} - F(r,\theta)C^n_{i,j-1}, \end{aligned} \tag{9}$$

$$\begin{aligned} A(r,\theta) &= \lambda_r\left[+\frac{\Delta r}{4}\left\{\frac{1}{r^+} - \alpha a E_0 \frac{eZ^*}{kT}\left(1 - \frac{1}{r^{+2}}\right)\cos\theta\right\}\right] \\ B(r,\theta) &= \lambda_r + \frac{\lambda_\theta}{r^{+2}} \\ D(r,\theta) &= \lambda_r\left[\frac{1}{2} - \frac{\Delta r}{4}\left\{\frac{1}{r^+} - \alpha a E_0 \frac{eZ^*}{kT}\left(1 - \frac{1}{r^{+2}}\right)\cos\theta\right\}\right] \\ E(r,\theta) &= \lambda_\theta\left[\frac{1}{2r^{+2}} + \frac{\Delta\theta}{4}\left\{\alpha a E_0 \frac{eZ^*}{kT}\left(\frac{1}{r^+} + \frac{1}{r^{+3}}\right)\sin\theta\right\}\right] \\ F(r,\theta) &= \lambda_\theta\left[\frac{1}{2r^{+2}} - \frac{\Delta\theta}{4}\left\{\alpha a E_0 \frac{eZ^*}{kT}\left(\frac{1}{r^+} + \frac{1}{r^{+3}}\right)\sin\theta\right\}\right]. \end{aligned} \tag{10}$$

Equation (9) is solved using the SOR method. An acceleration parameter of 0.8 is selected as the value of β in SOR, because the under-relaxation method ($0 < \beta < 1$) is useful to solve this nonlinear equation numerically.

3. Results and Discussion

3.1 Atom transport due to EM

The numerical analysis is conducted with current density $= 2.0 \times 10^{10}$ A/m^2 and absolute temperature $= 473$ K. Figure 3 shows the results for the behavior of atom transport by EM. The atom moves toward the anode end along an initial defect. Figure 4 shows a comparison between the results obtained by this numerical simulation and the analytical results under steady state conditions.[8] The atom distribution around an initial defect is analytically obtained in eq. (11).

$$C = C_0 \exp\left\{\frac{e|Z^*|}{kT}(\phi + \psi)\right\}. \tag{11}$$

Since the mathematical analysis was conducted for an equilibrium situation, Figure 4(a) shows the Cu atom distribution after a sufficient time has elapsed ($t+ =$ 22000 steps). Both results reveal that the maximum atom concentration occurs at the anode end and that the numerical result is valid from the transient state to the steady state.

3.2 The electric field dependence of Cu atom accumulation

Figure 5 shows the time-sequential change of atom concentration at the anode end with various current densities. The concentration of atoms and time are normalized by eq. (6). The rate of accumulation of atoms and the maximum concentration increase as current density increases. Figure 6 shows the time sequential change of normalized concentration of atoms at the anode end for various temperatures. It is obvious that the non-dimensional values of rate of accumulation of atoms and the maximum concentration are less influenced by temperature than by current density. The equation for atom transport due to EM, given in eq. (1), consists of a first term which indicates the diffusion, and a second term which indicates the accumulation. The electric field contributes only to the accumulation term, but temperature contributes to both diffusion and accumulation via the diffusion coefficient. The smaller influence of temperature is caused by the fact that the promotion of accumulation is compensated by the diffusion On the other hand, it is seen in Fig. 5 that electric field has a significant influence in promoting atom accumulation. Figure 7 shows the relation-

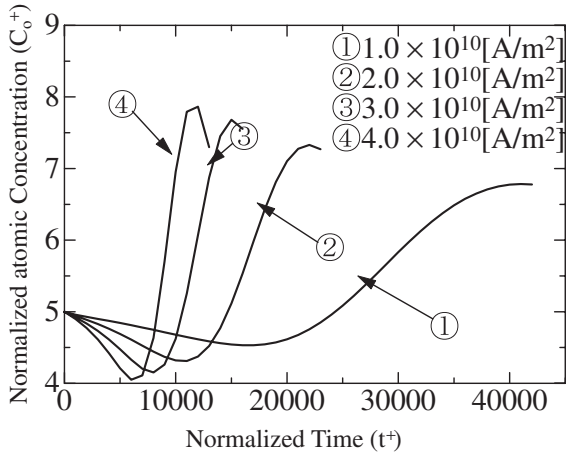

Fig. 5 The time sequential characteristics of the atomic concentration at the lower end of the anode for various values of electric current density.

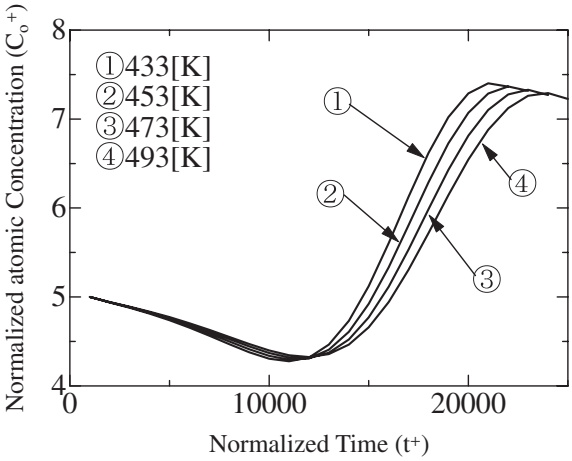

Fig. 6 The time sequential characteristics of the atomic concentration at the lower end of the anode for various values of temperature.

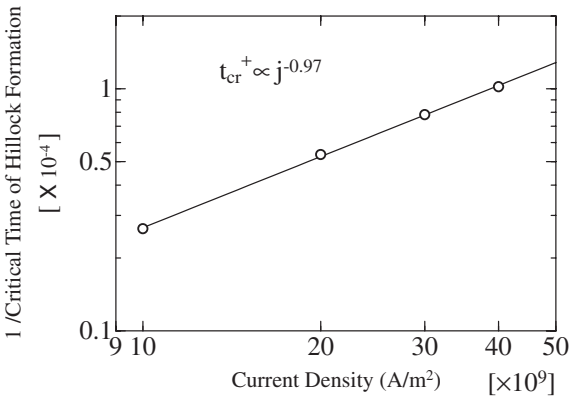

Fig. 7 The relationship between critical time for hillock formation, t_{cr}^{h+} and current density, j.

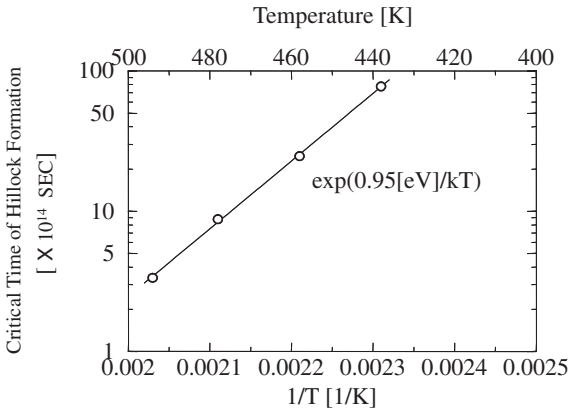

Fig. 8 The relationship between the critical time for hillock formation, t_{cr}^{h+} and temperature, T.

ship between the non-dimensional value of critical time for hillock formation and the current density. The non-dimensional critical time for hillock formation is defined as the time when the concentration of atoms reaches a certain critical value, $C = 6.7$ in this paper, at the anode end.

The non-dimensional critical time for hillock formation is formulated as shown in eq. (12).

$$t_{cr}^{h+} \propto j^{-0.97}. \tag{12}$$

Figure 8 shows the relationship between the non-dimensional value of the critical time for hillock formation and the temperature. According to eq. (6), the critical time for hillock formation is expressed by eq. (13).

$$t_{cr}^{h} \propto \exp\left(\frac{0.95[eV]}{kT}\right). \tag{13}$$

Then, the critical time for hillock formation is expressed shown in eq. (14).

$$t_{cr}^{h} \propto j^{-0.97} \exp\left(\frac{0.95[eV]}{kT}\right). \tag{14}$$

Since the activation energy in eq. (14) is almost equal to 1.0 eV, which is reported as that for Cu surface diffusion, the time for hillock formation is determined by Cu atom transport on the Cu surface.

3.3 The electric field dependence of void generation

The void generation is defined as the Cu atom depletion in eq. (15).

$$\eta = \text{void generation} = \frac{\text{initial Cu atom concentration} - \text{present Cu atom concentration}}{\text{Initial Cu atom concentration}} \times 100. \tag{15}$$

The non-dimensional value of the critical time for void generation is determined to be $\eta = 0.4$ in this report. Figure 9 shows the dependence of the non-dimensional value of the critical time for void generation on current density at the defect tip. The non-dimensional critical time for void generation is obtained from eq. (16).

$$t_{cr}^{v+} \propto j^{-0.92}. \tag{16}$$

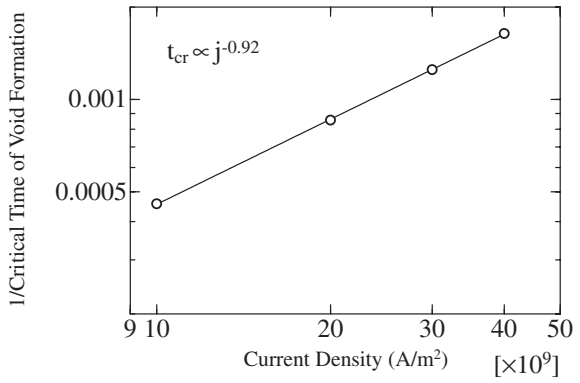

Fig. 9 The relationship between the critical time for void formation, $t_{cr}^{v}{}^{+}$ and the current density, j.

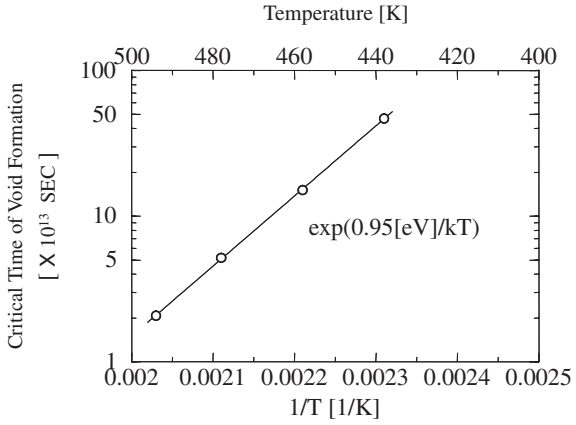

Fig. 10 The relationship between critical time of void formation, $t_{cr}^{v}{}^{+}$ and temperature, T.

Figure 10 shows the dependence of critical time for void generation on temperature. The critical time for void generation is expressed in eq. (17).

$$t_{cr}^{v} \propto j^{-0.92} \exp\left(\frac{0.95[eV]}{kT}\right). \tag{17}$$

Comparison of eq. (17) and eq. (14) shows that void formation and hillock formation can be described by the same physical model; Cu atom depletion at the defect tip results in void generation and Cu atom accumulation at the anode end results in hillock formation.

Black's equation, in eq. (18), is a well-known method for estimating EM lifetime.[10)]

$$TTF = Aj^{-n} \exp\left(\frac{Q}{kT}\right), \tag{18}$$

where *TTF* is the time to failure and *n* is the current density exponent, usually in the range $1 < n < 2$. *Q* is activation energy and usually takes a value of 1.0 eV in Cu line.

The current density exponent *n* is reported to be equal to 1 when the EM lifetime is determined by void growth.[11)] On the other hand, the current density exponent *n* is equal to 2 when the EM lifetime is determined by void nucleation. Since we consider void growth near to a defect, the current density exponent *n* is 1 in this study. Moreover, the results show that the numerical analysis is valid for the description of EM phenomena.

4. Conclusions

The following conclusions were obtained as a result of analyzing EM voiding with the numerical analysis:

(1) The result that atom concentration obtained by the numerical analysis after a long time passed was similar to that obtained by mathematical analysis demonstrates the validity of the numerical analysis.
(2) The Black's equation which was obtained from experimental result was derived by the numerical analysis.
(3) The mechanism of void generation at the notch tip is similar to that of hillock formation at the cathode end. The accumulation of vacancies and atoms behaves in "mirror image".

REFERENCES

1) *The International Technology Roadmap for Semiconductors*, (2003).
2) T. Nemoto and T. Nogami: *The 32nd annual Proceedings of Reliability Physics Symposium*, (1994) 207.
3) T. Nitta, T. Ohmi, T. Hoshi, S. Sakai, K. Sakaibara, S. Imai and T. Shibata: J. Electrochem. Soc. **140** (1993) 1131.
4) T. Nemoto and T. Nogami: 1995 International VLSI Multilevel Interconnection Conference, (1995) 362.
5) H. B. Huntington: *Diffusion in Solids*, (Academic Press, San Francisco, 1975), pp. 303.
6) K. Sasagawa, M. Hasegawa, M. Sala and H. Abe: Journal of Applied Physics **91** (2002) 1882.
7) M. R. Gungor and D. Maroudas: Journal of Applied Physics **85** (1999) 2233.
8) T. Nemoto, A. T, Yokobori, Jr. and T. Murakawa: Japan Journal of Applied Physics **45** (2006) 5716.
9) A. T. Yokobori, Jr., T. Nemoto, K. Sato and T. Yamada: Eng. Frac. Mech. **55** (1996) 47.
10) J. R. Lloyd: J. Phys. D. **32** (1999) 109.
11) Y.-J. Park, V. K, Andleigh and C. V. Thompson: J. Appl. Phys. **85** (1999) 3546.